

Material Quality Requirements for Intermediate Band Solar Cells

Matthew M. Wilkins , Eduard C. Dumitrescu , and Jacob J. Krich 

Abstract—Intermediate band (IB) solar cells hold the promise of efficiency as high as triple-junction solar cells with much simpler cell design, containing only two semiconductor material interfaces. Although several IB materials have been demonstrated, no cells have shown promising efficiencies. Many of the fundamental required properties of IB materials are well known; they need strong subgap absorption, long carrier lifetimes, and good carrier mobilities. The tradeoffs between these properties, however, are not well understood. We present the first results using a new coupled Poisson/drift-diffusion model designed for IB materials, called Simudo. We compare the results from Simudo to a simpler semianalytic model for IB device performance, highlighting where they agree well. Using both of these models, we perform a systematic study of a figure of merit for IB materials ν . We consider the standard p-IB-n architecture with a high-density IB, in which two depletion junctions are formed. Considering materials with identical electron and hole properties, we show that ν is well correlated with device efficiency. We show for the first time a threshold behavior, where the efficiency of the IB device exceeds that of the standard p-n-junction only for sufficiently high-quality material. We show that ν is similarly predictive of device performance as an equivalent figure of merit is for standard solar cells. These results both give guidance for experiments regarding required IB material properties and demonstrate how detailed device modeling can aid in the design of IB devices, for example, by choosing layer thicknesses optimally.

Index Terms—Charge carrier lifetime, mathematical model, photovoltaic cells.

I. INTRODUCTION

THE INTERMEDIATE band (IB) solar cell (IBSC) has the potential to provide the efficiency of a triple-junction solar cell with only two material interfaces, in addition to electrical contacts [1], [2]. An IB material is a standard semiconductor with a band of allowed electron energy levels deep inside the bandgap. The material can absorb two subgap photons to move an electron sequentially from valence band (VB) to IB to conduction band (CB). The standard IBSC device is a p-IB-n junction;

since no current is directly extracted from the IB, the voltage is set by the larger bandgap of the standard semiconductors. Achieving high efficiency requires IB materials with bandgaps appropriately matched to the solar spectrum, sufficiently strong subgap absorptions, and sufficiently long carrier lifetimes. The proven IB devices have efficiencies well below those predicted by detailed balance calculations, which ignore deleterious non-radiative recombination effects [2]–[6]. While it is not clear how high the efficiency of these devices could be if their junctions were perfect and layer thicknesses were chosen optimally, it is essential to determine when IB materials have sufficient quality to enable improved efficiency in IBSC devices.

In this work, we show that a simple figure of merit ν [7] for IB absorbers provides a necessary condition for efficient IBSC devices in the diffusive limit and that when bandgaps are held fixed, ν must be greater than a fixed value to achieve any increase in efficiency. Section II derives ν . Section III modifies an analytic model for JV curves of ideal IBSCs (i.e., in the radiative limit, with infinite mobility) [8] to include nonradiative trapping and carrier transport; we call this model the modified Strandberg model (MSM). Section IV presents the first study of any IB materials using the new coupled Poisson/drift-diffusion model, Simudo [9], [10], and shows the qualitative agreement of MSM to the full Simudo results. Section V uses the (computationally inexpensive) MSM to explore the relationship between ν and efficiency. It shows that ν is correlated with attainable IB device efficiency similarly to the way that a well known figure of merit for standard homojunction solar cells is correlated with attainable efficiencies. It also considers systems with a range of bandgaps and the required ν for high efficiency. These analyses show the power of ν for indicating required material properties for IBSCs and show how to optimize the IB layer thickness for best efficiency with fixed material quality.

This manuscript is an extended version of an IEEE Photovoltaic Specialists Conference Proceeding [11]. This version adds Sections III and V and compares the MSM and Simudo results in Section IV.

II. FIGURE OF MERIT FOR INTERMEDIATE BAND MATERIALS

The figure of merit ν is designed to capture the tradeoff between subgap absorption and carrier transport losses in IB devices. It was first proposed in [7], and we briefly rederive it here. Consider a one-dimensional (1-D) p-IB-n IBSC structure as in Fig. 1 in which the p- and n-type semiconductors are of good material quality, with strong optical absorption, long

Manuscript received July 28, 2019; revised October 22, 2019; accepted December 11, 2019. Date of publication January 17, 2020; date of current version February 19, 2020. This work was supported by the U.S. Army Research Laboratory under Cooperative Agreement W911NF-16-2-0167. (*Corresponding author: Jacob J. Krich.*)

M. M. Wilkins and J. J. Krich are with the Department of Physics and the School of Electrical Engineering and Computer Science, University of Ottawa, Ottawa, ON K1N 6N5, Canada (e-mail: mwilkin3@uottawa.ca; jkrich@uottawa.ca).

E. C. Dumitrescu is with the Department of Physics, University of Ottawa, Ottawa, ON K1N 6N5, Canada (e-mail: edumi042@uottawa.ca).

Color versions of one or more of the figures in this article are available online at <http://ieeexplore.ieee.org>.

Digital Object Identifier 10.1109/JPHOTOV.2019.2959934

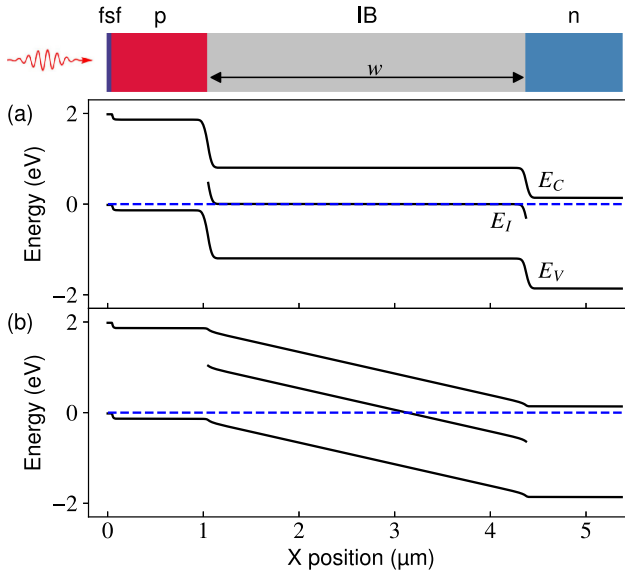


Fig. 1. Band diagrams of (a) diffusive- and (b) drift-limited p-IB-n devices at thermal equilibrium, produced by Simudo. Blue dashed lines indicate the Fermi energy. There is a 50 nm p++ front-surface field at the left.

diffusion lengths, and low surface recombination velocities; that is, potential problems with the device are due to the IB region alone. Electrons produced in the p-type emitter and both electrons and holes produced in the IB region must traverse the IB region, of width w , to reach their respective contacts.

An efficient IB material must both absorb a significant fraction of the subgap light and must have a large ratio of the lifetime of the electron or hole, τ_e or τ_h , respectively, to the transit time for the carrier through the IB region. Consider that the absorptivities of the two subgap transitions are α_{IV} and α_{CI} for the VB to IB and IB to CB transitions, respectively. For simplicity, we approximate those absorptivities as constants within the energy range available to the transitions. For Sections II and III, we further assume that all absorptivities are spatially constant, although we go beyond this approximation in Section IV. Then, the subgap optical depths are $OD_{IV} = w\alpha_{IV}$ and $OD_{CI} = w\alpha_{CI}$. An efficient IB device must have $\min[OD_{IV}, OD_{CI}] \equiv OD_{\min}$ of order 1, i.e., $w \approx 1/\alpha_{\min}$ for a device without light trapping.

In the case where the IB is of relatively high density and two depletion junctions are formed with the surrounding semiconductor material, as in Fig. 1(a), the electrons and holes must diffuse across the IB region. The mean time for them to traverse the IB region is

$$t_{tr,i} = \frac{w^2}{2D_i} = \frac{w^2 q}{2\mu_i k_b T} \quad (1)$$

where i can be either electron or hole, $D_i = \mu_i k_b T / q$ is the diffusion constant, which is connected by the Einstein relation to the carrier mobility μ_i , Boltzmann's constant k_b , temperature T , and electric charge q . In the case that $OD_{\min} = \sqrt{2}$ (chosen for numerical convenience), $t_{tr,i} = (k_b T \mu_i \alpha_{\min}^2 / q)^{-1}$. We thus find that the ratio of τ to t_{tr} is $\nu_i \equiv \frac{k_b T}{q} \mu_i \tau_i \alpha_{\min}^2$. Since ν_i must be large for both electrons and holes, the overall figure of merit

in the diffusive case is

$$\nu = \min_i(\nu_i) = \frac{k_b T}{q} \min_i(\mu_i \tau_i) \min_i(\alpha_i)^2 \quad (2)$$

which is expressed in this form for the first time. This figure of merit depends on properties of the IB absorber material alone and indicates the tradeoffs between nonradiative lifetimes and subgap absorptivity in real materials, helping to guide material development [12], [13].

In the low-IB-density limit, with appreciable electric fields in the IB region, as in Fig. 1(b), a similar derivation gives $\nu^{\text{drift}} = E_g (\mu \tau)_{\min} \alpha_{\min}^2 / q$, where E_g is the CB–VB bandgap of the IB region [14]. This result is of the same form as ν in (2) with the thermal energy $k_b T$ replaced by E_g . A structure with light trapping can have $OD \approx 1$ with $w \ll 1/\alpha_{\min}$, which can reduce the required value of ν by more than three orders of magnitude [14].

There has been a small number of studies measuring ν to date. In sulfur-hyperdoped silicon, ν_n^{drift} has been measured to be less than 0.5 [12], [13], and ν_p has not been measured. In the quaternary highly mismatched alloy GaPAsN, data sufficient to extract $\alpha_{\min} \approx 5000 \text{ cm}^{-1}$ and $\tau_{\min} = 23 \text{ ps}$ have been presented, where the CI process is both optically weaker and has shorter lifetime [15]. Since $E_g = 2.3 \text{ eV}$, an optimistic estimate of $\mu_n = 1000 \text{ cm}^2/\text{Vs}$ gives $\nu^{\text{drift}} \approx 1.3$. The results of Sections IV and V indicate that both of these systems are promising in IBSC architectures with some amount of light trapping, and the GaPAsN may not need much light trapping to make effective devices. There is need to measure ν in more IBSC candidate systems.

In the diffusive case, one can write ν in terms of the diffusion lengths $L_i = \sqrt{D_i \tau_i}$, so $\nu = (L_{\min} \alpha_{\min})^2$, where L_{\min} is the smaller of the electron and hole diffusion lengths in the IB material. We choose to use the expression in (2), as it keeps the same product of material parameters $\mu \tau \alpha^2$ as in the drift case. In Section V, we compare the predictive value of ν for IBSCs to $L\alpha$ for standard solar cells.

This analytical motivation of ν as a figure of merit does not indicate how large ν needs to be to achieve high efficiency. A previous semianalytic minority-carrier diffusion model for the IB indicated that $\nu \approx 1$ is required for an IBSC to be more efficient than the equivalent p-n-junction device with optimal bandgaps [16]. That model, however, did not include coupling between charge and transport or self-consistent optics, where the IB absorption varies with the IB filling fraction [17].

Here, we analyze the figure of merit using two models: 1) Simudo—a coupled Poisson/drift-diffusion solver including carrier transport in all three bands, nonradiative trapping and generation, and self-consistent optical generation, and 2) the semi-analytic MSM. Simudo is the first IB device modeling tool capable of treating all of these effects, which are essential for trustworthy simulations of new materials and devices. A large value of ν is a necessary but not sufficient condition for an efficient IBSC; to achieve high efficiency, an IBSC must have bandgaps well matched to the solar spectrum [1], [2], [18], [19]. We show in Section V that with well chosen bandgaps, high efficiency can be achieved with ν of $O(1)$ without light trapping,

while less optimal bandgaps require higher values of ν and/or light trapping.

III. MODIFIED STRANDBERG MODEL

Strandberg derived an analytic $J(V)$ for IBSCs making these assumptions [8]:

- 1) high mobility (i.e., electron, hole, and IB quasi-Fermi levels F_C , F_V , and F_I are spatially constant in the IB region);
- 2) radiative recombination only;
- 3) nondegenerate statistics in the VB and CB;
- 4) nonoverlapping absorption coefficients.

Assumption 1 implies that the external bias V equals $F_{CV} \equiv F_C - F_V$ throughout the IB region. Assumption 4 means that each photon can be absorbed by only one transition (either CV, CI, or IV), with no competition. Assumptions 2–4 together imply that the recombination flux [dimensions of (area time) $^{-1}$] originating from bands X and Y can be written as

$$R_{XY}^{\text{rad}} = R_{0,XY}^{\text{rad}} e^{qF_{XY}/k_b T} \quad (3)$$

where

$$R_{0,XY}^{\text{rad}} = 2\pi/h^3 c^2 \int a_{XY}(E) E^2 e^{-E/k_b T} dE \quad (4)$$

where h is Planck's constant, c is the speed of light, and a_{XY} is the absorptance, assumed to be constant for all energies absorbed in the XY transition [8]. As originally presented, a_{XY} was assumed to be 1 for all allowed photon energies.

Then, with generation rates G_{XY} , the system can be solved to give

$$J = J_G - J_{0,CV} e^{qV/k_b T} - \sqrt{J_{0,ib}^2 e^{qV/k_b T} + \frac{1}{4} \Delta J_{ib}^2} \quad (5)$$

where

$$J_G = q \left(G_{CV} + \frac{G_{CI} + G_{IV}}{2} \right) \quad (6a)$$

$$\Delta J_{ib} = q(G_{CI} - G_{IV}) \quad (6b)$$

$$J_{0,CV} = qR_{0,CV}^{\text{rad}} \quad (6c)$$

$$J_{0,ib} = q\sqrt{R_{0,CI}^{\text{rad}} R_{0,IV}^{\text{rad}}} \quad (6d)$$

Because of the high-mobility assumption, this model does not explicitly contain the width of the IB, although it can enter through the optical depth contributing to the generation rates G_{XY} . Equation (5) provides an easily evaluated model for IBSC JV curves.

We extend this model to include nonradiative Shockley–Read trapping to the IB and incomplete carrier collection due to that same recombination. We continue to use assumption 1 that the F_X are spatially constant and $V = F_{CV}$, even though this assumption is not consistent with less-than-unity carrier collection; we show in Section IV that this model works well despite these contradictory assumptions, but we would not be able to trust it without the Poisson/drift-diffusion modeling. This assumption enables $J(V)$ to retain the same form as (5), and Section IV shows that the resulting model remains qualitatively

accurate. Constant F_I implies that f , α_{CI} , and α_{IV} are all spatially constant.

A. Shockley–Read Trapping

Shockley–Read trapping from CB to IB under assumption 3 has a rate (per volume)

$$r_{CI} = c_n n (1 - f) - c_n n_1 f \quad (7)$$

where $c_n = \sigma_{CI}^{\text{th}} N_I v_{th,n}$ is the trapping rate, with N_I the density of traps, $v_{th,n}$ the CB thermal velocity, σ_{CI}^{th} the thermal capture cross section, n the CB carrier concentration, $f = 1/(\exp[q(E_I - F_I)/k_b T] + 1)$ is the trap (or IB) fill fraction where E_I is the IB energy, and n_1 is n when F_C is at the trap energy level [20]. We use the standard nondegenerate results that

$$n = N_c \exp[-q(E_C - F_C)/k_b T] \quad (8)$$

$$p = N_v \exp[-q(F_V - E_V)/k_b T] \quad (9)$$

where N_c , N_v are the CB and VB effective densities of states, respectively, and E_C , E_V are the CB and VB edge energies, respectively. With these expressions

$$r_{CI} = c_n n_1 f \left(e^{qF_{CI}/k_b T} - 1 \right) \quad (10)$$

and since we assume that F_{CI} is spatially constant, we can write the equivalent recombination flux $R_{CI}^{\text{SR}} = wr_{CI}$. The “−1” in the expression for r_{CI} corresponds to the thermal generation process, which is negligible in an illuminated system. Ignoring that term, as Strandberg does for the equivalent thermal generation, we see that R_{CI}^{SR} has the voltage dependence of (3) if f (or equivalently F_I) is independent of voltage, with $R_{0,CI}^{\text{SR}} = wc_n n_1 f$. Equivalently, we find $R_{0,IV}^{\text{SR}} = wc_p p_1 (1 - f)$.

We can combine the nonradiative and radiative processes in two ways. The simplest is to combine our existing results and write $R_{0,CI}^{\text{tot}} = R_{0,CI}^{\text{SR}} + R_{0,CI}^{\text{rad}}$ and equivalently for $R_{0,IV}^{\text{tot}}$. This method automatically includes photon recycling by considering only externally emitted photons. If we set the 1-pass absorptance to be $a_{XY} = 1 - \exp(-\alpha_{XY} w)$, we obtain the same w dependence for radiative and nonradiative processes when $\alpha_{XY} w \ll 1$ but a width-independent radiative loss when $\alpha_{XY} w \gg 1$. Although this method is the most accurate, if we seek agreement with a model, such as Simudo, that does not contain photon recycling, we can instead put the radiative process on a similar footing to the Shockley–Read trapping by writing the radiative recombination rates in the Shockley–van Roosbroeck form as [21]

$$c_n^{\text{rad}} = \frac{4n_r^2 \alpha_{CI}}{n_1} R_{0,CI}^{\text{rad}} \Big|_{\alpha_{CI} \rightarrow 1} \quad (11)$$

$$c_p^{\text{rad}} = \frac{4n_r^2 \alpha_{IV}}{p_1} R_{0,IV}^{\text{rad}} \Big|_{\alpha_{IV} \rightarrow 1} \quad (12)$$

where (4) is evaluated in the limit $a_{XY} = 1$ in the allowed energy interval and n_r is the index of refraction. This form allows us to write $R_{0,CI}^{\text{tot}} = w(c_n + c_n^{\text{rad}})n_1 f$ and $R_{0,IV}^{\text{tot}} = w(c_p + c_p^{\text{rad}})p_1 (1 - f)$. With either method, (6d) is replaced by

$$J_{0,ib} = q\sqrt{R_{0,CI}^{\text{tot}} R_{0,IV}^{\text{tot}}} \quad (13)$$

The $J_{0,CV}$ can similarly be replaced by the standard expression for a p-n-junction [22]

$$J_{0,CV} = qn_i^2 \left(\frac{D_n}{N_A L_n} \tanh(w_p/L_n) + \frac{D_p}{N_D L_p} \tanh(w_n/L_p) \right) \quad (14)$$

where n_i is the intrinsic carrier concentration, D_n , D_p are the electron and hole minority diffusion constants. In the following results, we consider the good-device limit that w_p/L_n and w_n/L_p are much less than 1.

B. Incomplete Carrier Collection

If we made no further amendments, (5) with the newly proposed values for the J_0 terms would predict a short-circuit current equal to J_G , independent of w . As described in Section II, as w becomes larger, we should not be able to collect all of the photogenerated carriers. Instead, each of the optical generation terms should be reduced to represent only the collectable carriers at short circuit, as

$$\begin{aligned} G_{CI} &= q\Phi_{CI}[1 - \exp(-\alpha_{CI}w)]\eta_{CI} \\ G_{IV} &= q\Phi_{IV}[1 - \exp(-\alpha_{IV}w)]\eta_{IV} \\ G_{CV} &= q\Phi_{CV}\eta_{CV} \end{aligned} \quad (15)$$

where Φ_{XY} is the incident photon flux in the energy range absorbable by transition XY, α_{XY} is assumed to be constant over all energies inside the absorbable range, and η_{XY} is the probability of the electron or hole produced by the transition to reach the appropriate junction (i.e., electrons to reach the IB-n junction and holes to reach the p-IB junction). We assume here a p-IB-n structure in which all of the above-gap light is absorbed in the p-type material, so there is no optical-depth reduction of G_{CV} .

The time t required to diffuse through a distance x can be approximated using the fundamental diffusion relation

$$\langle x^2 \rangle = 2D_n t. \quad (16)$$

If trapping into the IB is a Poissonian process, the probability of survival on moving a distance x is

$$P_n(x) = e^{-t/\tau_n} = e^{-x^2/2D_n\tau_n} = e^{-x^2/2L_n^2} \quad (17)$$

where the diffusion length for electrons in the IB region is $L_n = \sqrt{\tau_n D_n}$, and a similar result holds for holes with $n \rightarrow p$.

The easiest term to estimate is η_{CV} , as it represents the probability of an electron produced in the p-type region diffusing across the entire IB region to the n-type region. Then

$$\eta_{CV} = e^{-w^2/2L_n^2}. \quad (18)$$

For electrons produced by optical absorption inside the IB, we consider the case of a Beer-Lambert absorption profile with spatially constant absorptivity α_{CI} . Then, the probability of the electron being produced at position x is

$$p_n(x) = \alpha_{CI} \frac{e^{-\alpha_{CI}x}}{1 - e^{-\alpha_{CI}w}}. \quad (19)$$

TABLE I
BASELINE PARAMETERS FOR SIMUDO AND MSM

E_g	2.0 eV	N_C, N_V	$2 \times 10^{19} \text{ cm}^{-3}$
E_I	$E_V+1.2 \text{ eV}$	N_I	$2.5 \times 10^{17} \text{ cm}^{-3}$
T	300 K	$v_{\text{th},n}, v_{\text{th},p}$	$2.0 \times 10^7, 1.6 \times 10^7 \text{ cm/s}$
$\sigma_{CI}^{\text{opt}}, \sigma_{IV}^{\text{opt}}$	$3 \times 10^{-14} \text{ cm}^2$	$\sigma_{CI}^{\text{th}}, \sigma_{IV}^{\text{th}}$	$10^{-15} \text{ to } 10^{-20} \text{ cm}^2$
N_D, N_A	10^{17} cm^{-3}	μ_e, μ_h, μ_I	$500 \text{ cm}^2/\text{Vs}$

Electrons produced a distance x into the IB region must diffuse through a distance $w - x$ to reach the n-type region, so their survival probability is

$$\eta_{CI} = \int_0^w p_n(x) P_n(w-x) dx \quad (20)$$

which can be integrated to give

$$\eta_{CI} = \frac{\pi}{2} \alpha_{CI} L_n e^{(\alpha_{CI} L_n)^2/2} \times \frac{\text{erf}\left(\frac{\alpha_{CI} L_n}{\sqrt{2}}\right) - \text{erf}\left(\frac{\alpha_{CI} L_n - w/L_n}{\sqrt{2}}\right)}{e^{\alpha_{CI} w} - 1}$$

where erf is the standard error function.

Since the optical absorption is strongest near the p-IB junction, the survival probability for holes to reach the p-type region is larger than that for electrons. The analogous derivation gives

$$\eta_{IV} = \frac{\pi}{2} \alpha_{IV} L_p e^{(\alpha_{IV} L_p)^2/2} \times \frac{\text{erf}\left(\frac{(\alpha_{IV} L_p)^2 + \alpha_{IV} w}{\sqrt{2}\alpha_{IV} L_p}\right) - \text{erf}\left(\frac{\alpha_{IV} L_p}{\sqrt{2}}\right)}{1 - e^{-\alpha_{IV} w}}.$$

With care taken to ensure that the difference of erfs is evaluated accurately, the modifications of (15) allows (5) to capture the key physics of nonradiative recombination in diffusive IB materials, and (5) with the modifications of (13)–(15) constitute the MSM.

IV. SIMUDO SIMULATION AND RESULTS

In this first detailed study of ν , we consider the same limit as in [16]—a fictitious material with identical electron and hole properties in the diffusive limit. We simulate this system using Simudo, without the assumptions required for the derivations of the MSM in Section III, and compare the results from Simudo and MSM. The parameters used are in Table I. We consider the IB at a single energy level E_I with carrier mobilities μ_i , with i being e , h , and I for the electrons, holes, and IB electrons, respectively. The IB is treated using Fermi statistics while the VB and CB are treated with nondegenerate Boltzmann statistics. For notational convenience, we consider an IB whose number of electronic levels is given by a density N_I , as for example, given by deep-level dopants in a semiconductor. Both the optical absorption and Shockley-Read trapping processes self-consistently depend on the local IB filling fraction f . Then, $\alpha_{CI} = \sigma_{CI}^{\text{opt}} N_I f$, where σ_{CI}^{opt} is the optical absorption cross section; $\tau_e^{-1} = \sigma_e^{\text{th}} v_{\text{th},e} N_I (1-f)$, and $\tau_h^{-1} = \sigma_h^{\text{th}} v_{\text{th},h} N_I f$, where v_{th} is the thermal velocity. We assume nonoverlapping absorptions, where each photon can be absorbed only by the lowest energy process consistent with

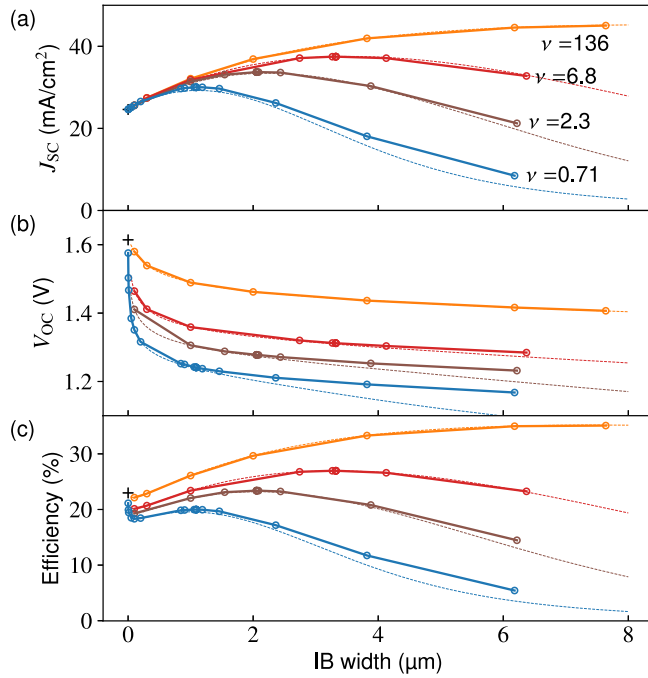


Fig. 2. IB device performance for varying figure of merit ν . (a) Short-circuit current density, (b) open-circuit voltage, and (c) power conversion efficiency. The limiting case of zero IB width is marked with a “+” symbol. Symbols show results of Simudo simulations, and solid lines are guides to the eye. Dotted lines show MSM results, which are not fits, using the same parameters.

energy conservation [1], and the σ_{XY}^{opt} are constant in space and energy, where they are nonzero. In order to focus on the properties of the IB material, the p- and n-type regions have long carrier lifetimes and are optically thick, 1 μm long, and there is a 50-nm front-surface field (fsf) region at the top of the p-type region, where the absorption is zero. We consider the 6000-K 1-sun blackbody spectrum. Our choice of bandgap and IB energetic position is purposely not optimal for IB devices, with the IV transition having approximately 1.5 times as many photons available as the CI transition. We consider the case where the charge-neutral filling of the IB is $f_0 = 1/2$ [1]. As Simudo does not model photon recycling, we set $n_r = 1$, to ensure that light trapping and photon recycling are negligible. For the calculation of depletion width, we use a value of static relative permittivity, $\varepsilon = 11.8$, which is typical of semiconductor materials but inconsistent with the refractive index. We make these same assumptions for n_r and ε in all other models as well.

In this study, we do not assume that OD = 1 but rather optimize w to find the maximum efficiency for each considered set of material parameters. Our goal is to find the maximum efficiency possible for a given material quality. We fix α_{XY} using σ_{XY}^{opt} in Table I and vary ν by changing σ^{th} .

Fig. 2(a) shows J_{sc} as a function of w for different material qualities. The baseline current of 24.6 mA/cm² arises from the p-n-junction alone, and as w increases, the IB region is able to absorb more of the subgap light. As w increases too far, t_{tr} exceeds τ , and the current begins to decline. Fig. 2(b) shows that V_{oc} declines with w for all material qualities. These two effects imply that ν must be larger than some threshold value ν_0

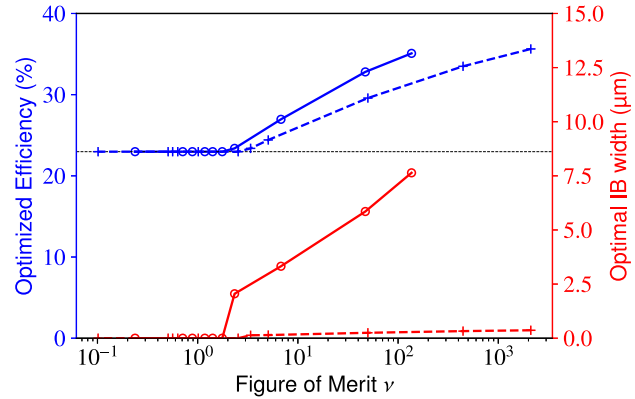


Fig. 3. Results of optimizing the IB region width. Optimized efficiency (blue, left axis) and optimal IB width (red, right axis). Circles show the data from Fig. 2. For $\nu < 2$, the device is best without an IB region. Crosses show a similar study with σ^{opt} increased to $8 \times 10^{-13} \text{ cm}^2$. With the larger absorptivity, the optimal widths are much smaller, as expected, and the critical value of ν has increased slightly to three. Lines are guides to the eye.

in order to obtain an improvement over the p-n-junction device. This effect is visible in Fig. 2(c), where the peak efficiency at finite w exceeds the 23.0% value at $w = 0$ only for $\nu > \nu_0$. For these parameters, $\nu_0 \approx 2$. This threshold behavior was not seen in the previous, less-sophisticated study [16] and is an important new result. The same threshold behavior is seen inside the MSM, which is shown with the dotted lines of Fig. 2, ignoring photon recycling in order to best match the Simudo results. Those curves are not fits but rather use $f = 1/2$ and the same parameters as in Table I in the MSM of Section III. Simudo and the MSM agree qualitatively in all cases and quantitatively for the high-quality materials. For lower quality materials, the MSM is slightly pessimistic in both current and voltage as w increases but in close agreement about the width-optimized efficiency and associated w . We conclude that the MSM is a good model for studying IBSCs in the high-mobility limit, which we consider further in Section V.

Taking the optimal w for each ν gives the efficiencies shown in Fig. 3. With $f = 1/2$, $\alpha_{CI} = \alpha_{IV} = 0.375 \mu\text{m}^{-1}$, so the width-optimized OD for $\nu > \nu_0$ is indeed of order 1, as assumed in the derivation of ν .

We ran a similar analysis with $\sigma_{CI}^{\text{opt}} = \sigma_{IV}^{\text{opt}}$ increased to $8 \times 10^{-13} \text{ cm}^2$, with ν again varied by changing σ^{th} , with the results shown with crosses in Fig. 3. In that case, the optimal IB widths are much smaller, owing to the increased subgap absorptivities, but the threshold value ν_0 increases only slightly to 3. For $\nu > \nu_0$, the efficiency is different than that in the case of smaller σ^{opt} , showing that there is no direct mapping from ν to efficiency, even with fixed band energies. The definition of ν is designed to indicate when good photocarrier collection is possible; however, the efficiency of a solar cell also depends on voltage, which introduces a further dependence on τ . In Fig. 3, the case with larger σ^{opt} has smaller τ at a given ν , and hence, lower efficiency. In other words, the figure of merit ν provides a necessary condition for high efficiency, but it does not provide the efficiency itself.

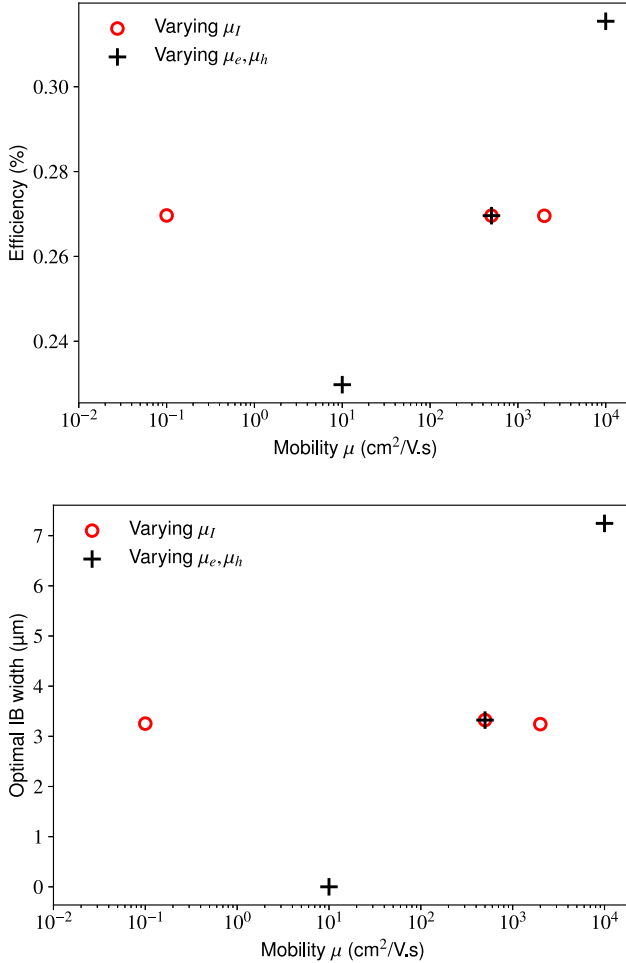


Fig. 4. Where Fig. 3 varies ν by changing σ^{th} , here we vary either $\mu_{e,h}$ (black symbols) or μ_I (red symbols), with all other parameters as in Fig. 2 with $\nu = 6.8$. Top panel shows the width-optimized efficiency and bottom panel shows the optimal width of the IB region. Consistent with the prediction of the figure of merit, changing μ_e, μ_h changes ν and also the optimal efficiency, while changing μ_I (which does not appear in ν) has no effect.

The figure of merit ν depends on the mobilities of the electrons and holes but does not depend on transport in the IB. While Figs. 2 and 3 vary ν by changing σ^{th} , changing the nonradiative trapping rates, we can test the accuracy of ν by varying the mobility instead. In this test case, with identical electron and hole properties, ν is proportional to $\mu_e = \mu_h$ but is independent of μ_I . Fig. 4 shows that varying $\mu_e = \mu_h$ with μ_I constant (black symbols) changes the optimal IB width and device efficiency, as we would expect. When $\mu_e = \mu_h = 10^4$ cm²/Vs, we have $\nu = 136$, but the width-optimized efficiency is 31.5% rather than the 35% shown in Fig. 2(c) at the same value of ν . Again, there is no direct mapping from ν to efficiency.

Changing μ_I (red symbols), however, has essentially no effect on the optimal widths or efficiencies, indicating that transport in the IB is unimportant to the operation of this model device. In the case that σ_{CI}^{opt} and σ_{IV}^{opt} are not identical, μ_I can be important for efficiency, as IB transport becomes important for current-matching in the IB, as discussed in [9, Sec. 5.3].

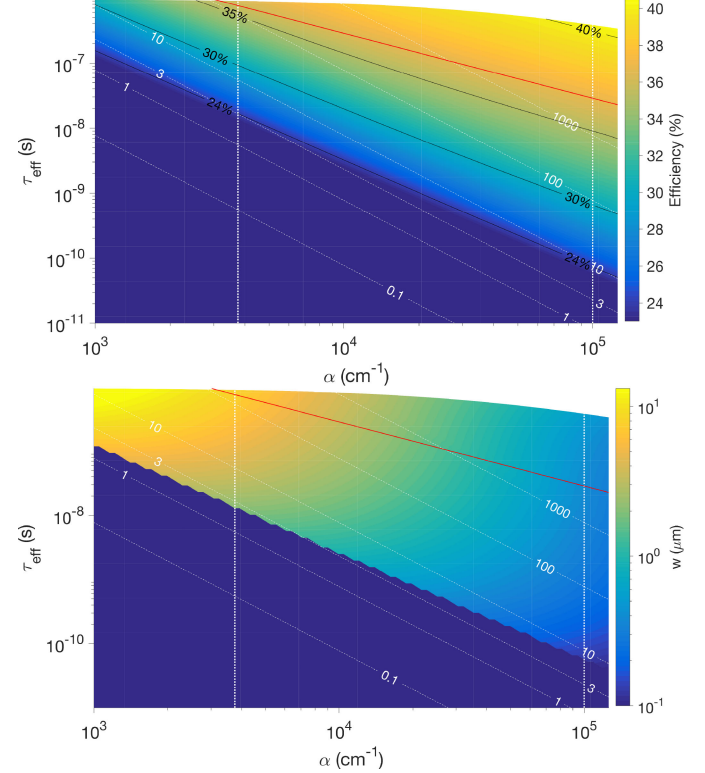


Fig. 5. (Top) Optimized efficiency in the MSM for an IBSC with band energies and mobilities as in Table I, for a variety of subgap absorptivities α and effective lifetimes in the IB region τ_{eff} , which include both radiative and nonradiative rates. White dashed contours show ν , calculated using τ_{eff} . Black solid contours show device efficiency. Vertical dotted lines show the two values of subgap α considered in Fig. 2. (Bottom) Width of IB at optimum efficiency, for the cases shown at top. Solid red line shows the radiative limit for τ without photon recycling

V. FROM FIGURE OF MERIT TO EFFICIENCY

The results summarized in Fig. 3 show that while efficiency increases with $\nu > \nu_0$, efficiency is not a function of ν ; different combinations of α and τ with the same ν give different width-optimized efficiencies. In this section, we use the MSM to show the full dependence of optimized efficiency on changes in τ and α , showing that ν is well correlated with efficiency but not perfectly predictive. We compare this result to the analogous situation of a standard p-n-junction solar cell, using an analytic model for homojunctions [23], sometimes called the Hovel model [24]. We show that the figure of merit αL is correlated with efficiency but not perfectly predictive, similarly to ν in the considered cases. We further show how the required ν for high efficiency varies as E_g and E_I change. We continue to consider a range of hypothetical materials with identical electron and hole properties.

Using the MSM, we consider a system with the same parameters as in Table I with $f = 1/2$ but vary $\alpha_{CI} = \alpha_{IV}$ and $\tau_e = \tau_h$. We include radiative effects using the method that incorporates photon recycling, with results shown in Fig. 5. As before, the input spectrum is a 1-sun blackbody, and the two transitions are not current matched. For each set of material parameters, we

vary the IB width to find the optimal efficiency. The effective lifetime is defined to be $\tau_{\text{eff}} = (c_n + \alpha_{CI} R_{0,CI}^{\text{rad}}/n_1)^{-1}$, with $R_{0,CI}^{\text{rad}}$ evaluated at the optimal width. If we did not include photon recycling, the figures would be essentially unchanged where $\nu < 10$, but the maximum achievable τ_{eff} would be considerably smaller, limiting the maximum efficiency to 36%, where 40% is attainable with photon recycling. The red curves in Fig. 5 indicate the maximum τ attainable without photon recycling.

Focusing on the lower quality portion of the figure, it is clear that ν is strongly correlated with device efficiency, but the contours of ν and η are not parallel, indicating that η is not simply a function of ν . Near ν_0 , the contours are close to parallel, indicating that ν is a good predictor for the threshold, where an IB material can begin to make a good device. For the two values of subgap α studied in Fig. 2, the MSM predicts values of ν_0 of 2.3 and 7.0, which compare to the Simudo-determined values of 2 and 3. In both cases, the MSM is a little more pessimistic than the full device simulation.

We now consider the case of a p-n-homojunction solar cell with the same bandgap, doping, and mobility as in Table I, studied using the depletion approximation and the analytic form in [23, Ch. 4], also known as the Hovel model. We consider minority carrier surface recombination velocities to be zero. We consider varied absorption coefficient α_{CV} and nonradiative minority carrier lifetime τ_{nr} . We include the radiative lifetime implied by α_{CV} , which does not include photon recycling effects [21]. When the material quality is high, this set of approximations is pessimistic, as the lifetime becomes radiatively limited but photon recycling is not included in this simple model. As in the other simulations, we set $n_r = 1$ to reduce this effect.

One important figure of merit for standard p-n-junction solar cells is the product $L\alpha_{CV}$, where L is the minority carrier diffusion length. In the case of diffusive IBSCs, as considered in this manuscript, $\nu = (L_{\min}\alpha_{\min})^2$, as noted in Section II. We consider the Hovel model for a variety of different τ_{nr} and α_{CV} , shown in Fig. 6. For each set of parameters considered, we fix the widths of both the n- and p-type regions to be equal, and vary them to find the optimal efficiency.

At very low efficiency, the two sets of contours in Fig. 6 are close to parallel, indicating that the efficiency can almost be written as a function of $L\alpha_{CV}$, but as the material quality improves, the sets of contours become less parallel, just as in Fig. 5. The comparison of Figs. 5 and 6 shows that the figure of merit ν for IBSCs behaves similarly to the figure of merit $L\alpha_{CV}$ for standard p-n-junction solar cells. Both are correlated with efficiency, but the efficiency is not a function of either figure of merit, even for systems with fixed bandgap.

When E_g and E_I change, device efficiency varies even with constant ν , because of the changing optical fluxes available to each transition. This effect is shown in Fig. 7, where we have varied the CB–VB bandgap E_g while holding the relative position of the intermediate band constant at $0.6E_g$ and fixed $\alpha_{CI} = \alpha_{IV} = 0.375 \mu\text{m}^{-1}$. The dashed line indicates the ν_0 threshold. We are not sweeping through the true optimum detailed balance bandgaps for IBSC at 1 sun, which occur at $E_g = 2.41 \text{ eV}$ and $E_I = 1.49 \text{ eV}$ [19], which have $E_I = 0.62E_g$. For given values of E_g and E_I , ν_0 provides an internal reference for when an IBSC

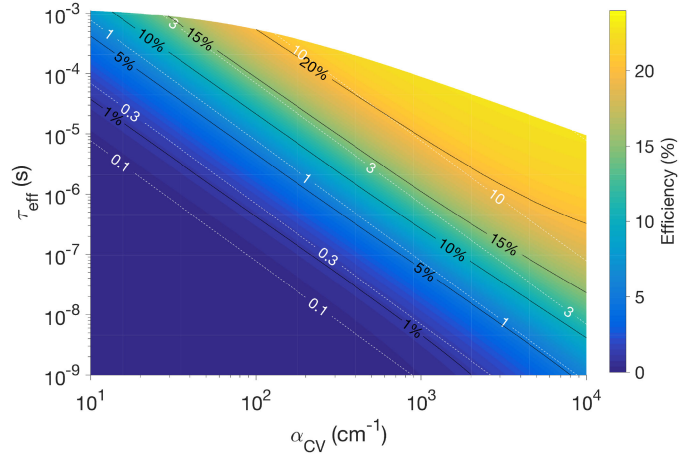


Fig. 6. Optimized efficiency in the Hovel model for a symmetrally doped p-n-homojunction solar cell with identical electron and hole properties. Vertical axis shows effective lifetime, including both radiative and nonradiative lifetimes. The white region in the upper right is unobtainable, as τ_{eff} is limited by τ_{rad} . White dashed contours show $L\alpha_{CV}$, with diffusion length L calculated using the effective lifetime τ_{eff} . Black solid contours show device efficiency.

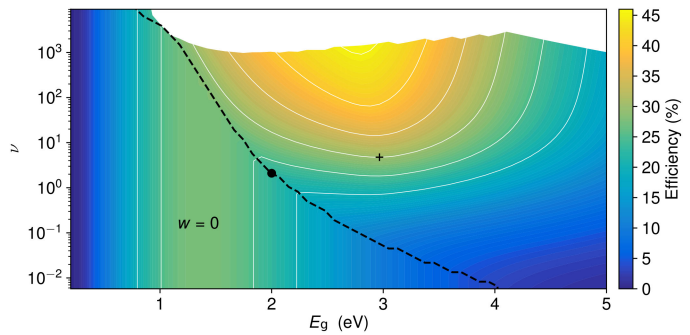


Fig. 7. Efficiency from the MSM with ν varied by changing τ_{nr} and varying CB–VB bandgap E_g with $E_I = 0.6E_g$. The dashed line indicates where an IB device is more efficient than a comparable device without an IB region (i.e., with $w = 0$). The black • represents ν_0 for the 2.0-eV material discussed throughout this article. The black '+' indicates the lowest value of ν where efficiency exceeds 30%. Calculations do not use photon recycling.

can be more efficient than the equivalent p-n-junction device. For E_g between 1 and 2 eV, where single-junction devices are at their most efficient and IBSC devices at 1 sun are not at their optimum, ν_0 is relatively larger. With larger E_g , the single-junction device becomes less efficient, and with that fixed E_g , the IBSC can be more efficient even with relatively small ν . Fig. 7 shows that achieving truly high efficiencies (e.g., 30% at 1 sun) requires ν to be greater than 4.8 for these combinations of bandgaps, with the ν required to achieve 30% efficiency increasing as the bandgaps move away from optimality.

VI. CONCLUSION

This article represents three significant advances for the field of IB materials. First, it confirms the value of the figure of merit ν in the diffusive case in predicting the potential improvements an IB material can make to a solar cell. Since the components of ν are measurable properties of an IB absorber alone, ν_0 provides

guidance on when a new material is sufficiently high quality to produce improvements to device efficiency. Second, it demonstrates the power of Simudo, the coupled Poisson/drift-diffusion solver, including intermediate band effects. Using Simudo, we can evaluate ν with more sophistication than has been previously achieved, and we can design optimal devices, giving clear guidance as to the optimal width for IB regions in devices. Finally, we have shown how to modify the Strandberg semianalytic model to include nonradiative processes, giving a flexible and easily evaluated model for theoretical study of IBSCs in the diffusive limit. Using Simudo, we have validated that this simple model provides qualitatively and almost quantitatively reliable results for many systems.

ACKNOWLEDGMENT

The authors would like to thank Compute Canada for computing resources.

REFERENCES

- [1] A. Luque and A. Martí, "Increasing the efficiency of ideal solar cells by photon induced transitions at intermediate levels," *Phys. Rev. Lett.*, vol. 78, no. 26, pp. 5014–5017, 1997.
- [2] Y. Okada *et al.*, "Intermediate band solar cells: Recent progress and future directions," *Appl. Phys. Rev.*, vol. 2, no. 2, 2015, Art. no. 021302.
- [3] W. Wang, A. S. Lin, and J. D. Phillips, "Intermediate-band photovoltaic solar cell based on ZnTe:O," *Appl. Phys. Lett.*, vol. 95, no. 1, 2009, Art. no. 011103.
- [4] N. López, L. A. Reichertz, K. M. Yu, K. Campman, and W. Walukiewicz, "Engineering the electronic band structure for multiband solar cells," *Phys. Rev. Lett.*, vol. 106, no. 2, 2011, Art. no. 028701.
- [5] K. S. Lee, G. Oh, D. Chu, S. W. Pak, and E. K. Kim, "High power conversion efficiency of intermediate band photovoltaic solar cell based on Cr-doped ZnTe," *Sol. Energy Mater. Sol. Cells*, vol. 170, pp. 27–32, 2017.
- [6] T. Tanaka, K. Saito, Q. Guo, K. M. Yu, and W. Walukiewicz, "Improved photovoltaic properties of ZnTeO-based intermediate band solar cells," *Proc. SPIE*, vol. 10527, 2018, Art. no. 105270P.
- [7] J. J. Krich, B. I. Halperin, and A. Aspuru-Guzik, "Nonradiative lifetimes in intermediate band photovoltaics—Absence of lifetime recovery," *J. Appl. Phys.*, vol. 112, no. 1, 2012, Art. no. 013707.
- [8] R. Strandberg, "Analytic JV-characteristics of ideal intermediate band solar cells and solar cells with up and downconverters," *IEEE Trans. Electron. Devices*, vol. 64, no. 5, pp. 2275–2282, May 2017.
- [9] E. C. Dumitrescu, M. M. Wilkins, and J. J. Krich, "Simudo: a device model for intermediate band materials," *J. Comput. Electron.*, pp. 1–17, 2019, doi: [10.1007/s10825-019-01414-3](https://doi.org/10.1007/s10825-019-01414-3)
- [10] E. C. Dumitrescu, M. M. Wilkins, and J. J. Krich, "Device model for intermediate band materials," in *Proc. IEEE 46th Photovolt. Spec. Conf.*, 2019.
- [11] M. M. Wilkins, E. C. Dumitrescu, and J. J. Krich, "Minimum material quality threshold for intermediate band solar cells using a multi-band device simulator with fully coupled optics," in *Proc. IEEE 46th Photovolt. Spec. Conf.*, 2019.
- [12] J. T. Sullivan *et al.*, "Methodology for vetting heavily doped semiconductors for intermediate band photovoltaics: A case study in sulfur-hyperdoped silicon," *J. Appl. Phys.*, vol. 114, no. 10, 2013, Art. no. 103701.
- [13] M.-J. Sher *et al.*, "Picosecond carrier recombination dynamics in chalcogen-hyperdoped silicon," *Appl. Phys. Lett.*, vol. 105, no. 5, 2014, Art. no. 053905.
- [14] J. T. Sullivan, C. B. Simmons, T. Buonassisi, and J. J. Krich, "Targeted search for effective intermediate band solar cell materials," *IEEE J. Photovolt.*, vol. 5, no. 1, pp. 212–218, Jan. 2015.
- [15] J. N. Heyman *et al.*, "Carrier lifetimes in a III–V–N intermediate-band semiconductor," *Phys. Rev. Appl.*, vol. 7, 2017, Art. no. 014016.
- [16] J. J. Krich, A. H. Trojnar, L. Feng, K. Hinzer, and A. W. Walker, "Modeling intermediate band solar cells: A roadmap to high efficiency," *Proc. SPIE*, vol. 8981, 2014, Art. no. 898100.
- [17] R. Strandberg and T. W. Reenaas, "Photofilling of intermediate bands," *J. Appl. Phys.*, vol. 105, no. 12, 2009, Art. no. 124512.
- [18] A. S. Brown and M. A. Green, "Impurity photovoltaic effect: Fundamental energy conversion efficiency limits," *J. Appl. Phys.*, vol. 92, no. 3, pp. 1329–1336, 2002.
- [19] A. Krishna and J. J. Krich, "Increasing efficiency in intermediate band solar cells with overlapping absorptions," *J. Opt.*, vol. 18, no. 7, 2016, Art. no. 074010.
- [20] W. Shockley and W. T. Read, "Statistics of the recombinations of holes and electrons," *Phys. Rev.*, vol. 87, no. 5, pp. 835–842, 1952.
- [21] W. van Roosbroeck and W. Shockley, "Photon-radiative recombination of electrons and holes in germanium," *Phys. Rev.*, vol. 94, no. 6, pp. 1558–1560, 1954.
- [22] J. Nelson, *The Physics of Solar Cells*. London, U.K.: Imperial College Press, 2003.
- [23] S. Fonash, *Solar Cell Device Physics*. 2nd ed. Burlington, MA, USA: Academic, 2010.
- [24] H. Hovel, *Solar cells* (Semiconductors and Semimetals, vol. 11), R. Willardson and A. Beer, Eds., New York, NY, USA: Academic, 1975.